This project has received funding from the European Union's Horizon 2020 research and innovation programme under under FET-Open grant agreement no. 899646 (k-NET)

DELIVERABLE

Project acronym	k-NET
Project full title	k-space neural computation with magnetic excitations
Grant Agreement no.	899646

Document title	**Deliverable 1.1 – Report on the design and fabrication of the first generation of k-NN hardware**
Revision no.	2
Document date	30/08/2021
Dissemination level	Confidential
Responsible partner	CEA
Contributing partners	CEA, CNRS, WWU, CESIC
Reviewing partners	All

CHANGE RECORD

Revision	Date	Changes	Authors	Status
2	30/08/2021	Polishing	G. de Loubens A. Anane, J. Ben-Youssef, M. Munoz V. Demidov T. Devolder	Submitted
1	25/08/2021	Version 1		Not submitted
	20/08/2021	First draft		

TABLE OF CONTENTS

1 SUMMARY

k-NET will pursue the objective of engineering spin-waves (SW) eigenmodes representing small collective oscillations of the magnetization around the equilibrium configuration of a ferromagnetic medium. In confined geometries, SW modes are quantized (i.e., only certain wavevectors are allowed in k-space), resulting in a discrete frequency spectrum. In the linear regime, SW modes can be considered as independent oscillators. However, the various interactions in ferromagnets can be described by an appropriate effective field, which itself depends on the magnetization, making SW dynamics, for sufficiently large deviations from the ground state, highly nonlinear. These intrinsic nonlinearities naturally couple the SW oscillations together. The objective of k-NET is to provide a proof of concept where this ensemble of discrete excitation modes (neurons) and their mutual couplings (synapses) are used as hardware for k-space based Neural Computing (k-NC). The control of the synaptic weights in this hardware can be achieved because nonlinear interactions between SW modes are predominantly determined by their amplitudes. Namely, the state of the system of SW modes, which can be controlled by external signals, defines how the energy (information) is channelled between different modes (neurons) by the nonlinearities (synapses). This enables programming the neural network (NN). Achieving this objective will require the fabrication and the optimization of devices and their characterization using three spectroscopic techniques.

- Micro-focussed Brillouin light spectroscopy (μ-BLS)

- Magnetic resonance force microscopy (MRFM)

- Vector network analyser based spectroscopy (VNA)

The two first methods (μ-BLS and MRFM) are highly sensitive techniques that can map the spin wave modes in reciprocal space (frequency, wave vector). They are however laboratory scale experiments. The third technique will mostly be relevant for practical implementation of the k-NC proof of concept. It has the best frequency and time resolution even if its sensitivity is less (relatively to that μ-BLS and MRFM).

The devices design has been pursued to obtain a coherent set of data on the SW eigenmodes. This choice is relevant as the different techniques have non-overlapping capabilities and will deliver complementary information. By maximizing completeness of the k-space mapping, a more reliable and accurate theoretical modelling (WP3) can be reached. Given the risk that slight variation from sample to sample of the magnetic properties and in particular the Gilbert damping parameter might exist, we decided that the three spectroscopy techniques should be conducted on the same garnets films. Requirements for such devices are high quality fabrication of YIG microstructures and interfacing such microstructures with radiofrequency excitation-detection circuitry. It is essential that the microfabrication process does not deteriorate the dynamical properties of the magnetic elements.

Yttrium Iron Garnet (YIG) has a small magneto-optical activity, it is small at all wavelengths with however an optimum at the blue wavelength (432 nm). As μ-BLS sensitivity is proportional to the films' Faraday effect, probing films that are sub-100 nm thick normally requires to use a blue probing laser, while BLS hardwares have optimal performances at the green (532 nm) lasers. In order to explore the possibility to optimize the μ-BLS response we explored substituting YIG with Bismuth (on the Yttrium site). We therefore also report here on this particular study.

This report is organised in 2 parts:

i/ Films fabrication and characterisation and ii/ microfabrication process description.

2 FILM GROWTH AND FILM SCALE CHARACTERIZATIONS

2.1 Growth of garnet films for device fabrication

Requirements for garnet films for k-NC as proposed by k-NET are the following:

1- Films should have an in-plane easy magnetization configuration to maximize ellipticity and hence inter-mode coupling.
2- Films should be relatively thick while preserving compatibility with standard microfabrication techniques.
3- Gilbert damping should be as small as possible to ensure long-living magnetic excitations.

A campaign of Liquid Phase Epitaxy (LPE) growth has been conducted using GGG (111) 1 inch substrates. The best films were selected and show the following characteristics.

THICKNESS: 66 nm obtained through X-ray reflectometry measurements (Figure 1).

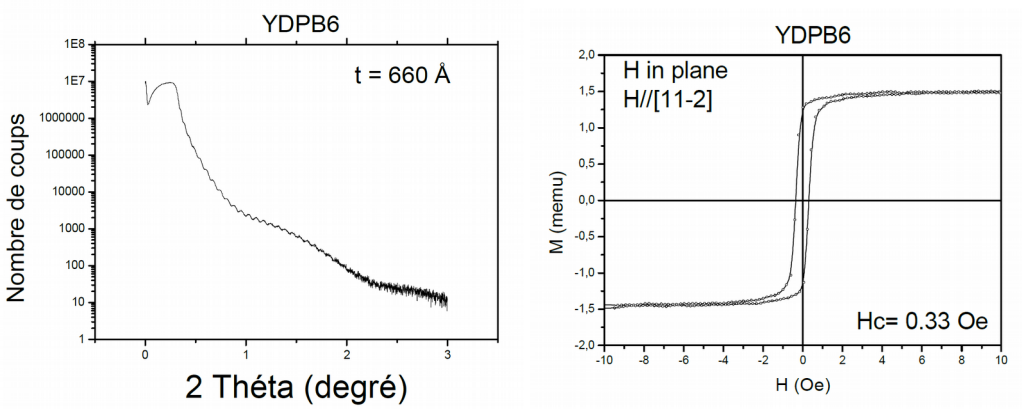

Figure 1: left panel: X-ray reflectometry showing a large number of oscillations which is a good indication of the low roughness and the large scale flatness of the film. Fitting to standard reflectometry models yields a film thickness of 66 nm. Right Panel, in-plane magnetization hysteresis curve measured at room temperature along the (11-2) crystallographic axis. The deduced magnetisation corresponds to the expected value for YIG. The squareness of the curve together with the extremely small hysteresis field points to the small density pinning sites affecting the domain wall dynamics during the switching process.

MAGNETIZATION: has been measured using VSM and is at the expected value for YIG ($\mu_0 M_s \sim$ 180 mT). The film also shows a square-like hysteresis (field is within the plan of the film along the (11-2) crystallographic axis). The small coercitive field (33µT) indicates also the high film quality (Figure 1).

FMR: This film has been characterized using broadband FMR up to 40 GHz. The fit to the Kittel equation yields an effective magnetization of $\mu_0 M_{eff}$ =176.8 mT, very close to the magnetization measurements. The out-of-plane magnetic anisotropy of this film is negligible.

The most important characteristic of this film is its Gilbert damping, obtained by fitting the frequency dependence of the peak-to-peak linewidth of the absorbed power derivative, $\Delta H_{pp}^{\square}(f)$, using equation 1:

$$\Delta H_{pp}^{\square} = \Delta H_0^{pp} + \frac{\frac{2}{\sqrt{3}} 2\pi\alpha f}{\gamma}$$

where ΔH_0^{pp} is the inhomogeneous broadening, a phenomenological parameters that accounts for film defects and large scale inhomogeneities, and γ the gyromagnetic ratio. The Gilbert damping parameter is $\alpha = 7.5\,10^{-5}$, this value is obtained from a least squares fitting method over the entire frequency range. Three conclusions can be drawn:

- The value of the Gilbert damping is the smallest ever observed on sub-100 nm thick YIG films. The total linewidth is also quite small (ranging from 0.1 mT to 0.4 mT).
- There is no noticeable deviation from the expected linear dependence of $\Delta H_{pp}^{\square}(f)$ up to 40 GHz. We, hence, do not see evidence for two-magnon scattering processes.
- The inhomogeneous broadening is only about 0.1 mT, which is evidence for the high quality of the structural and magnetic properties of the film.

This film is used to process the first generation of devices as will be described hereafter (section 3).

2.2 Growth of Bi:YIG films for large Magneto-optical response

2.2.1 Growth and FMR characterisations:

Bi substitution on the Yttrium site in YIG is well known to increase the magneto-optical effect (the Faraday rotation) while not deteriorating the FMR linewidth. We explored the possibility to slightly dope YIG and observe if the BLS signal is improved. To this intent a series of films have been fabricated using LPE. Bi content was intended to be small ($\leq$0.2 atoms per formula unit). Broadband FMR has been conducted and shows that indeed Bi does not affect significantly the FMR linewidth. Figure 2 shows four of those films as an illustration. We observe an increase of the Gilbert damping ranging from 10% to 100% subsequently to Bi doping. The Bi content is increasing with film label number (YIGB8, YIGB9 …) There is however no characterisation to quantify precisely the Bi content in each film.

2.2.2 BLS measurements of Bi doped YIG

Measurements of the thermal spectrum have been conducted using a blue laser and a green laser. Experimental measurement conditions have been set to be comparable (laser power, averaging time, frequency span). The goal of these measurements is to conclude on the added value in terms of sensitivity and laser wavelength in using Bi doped films.

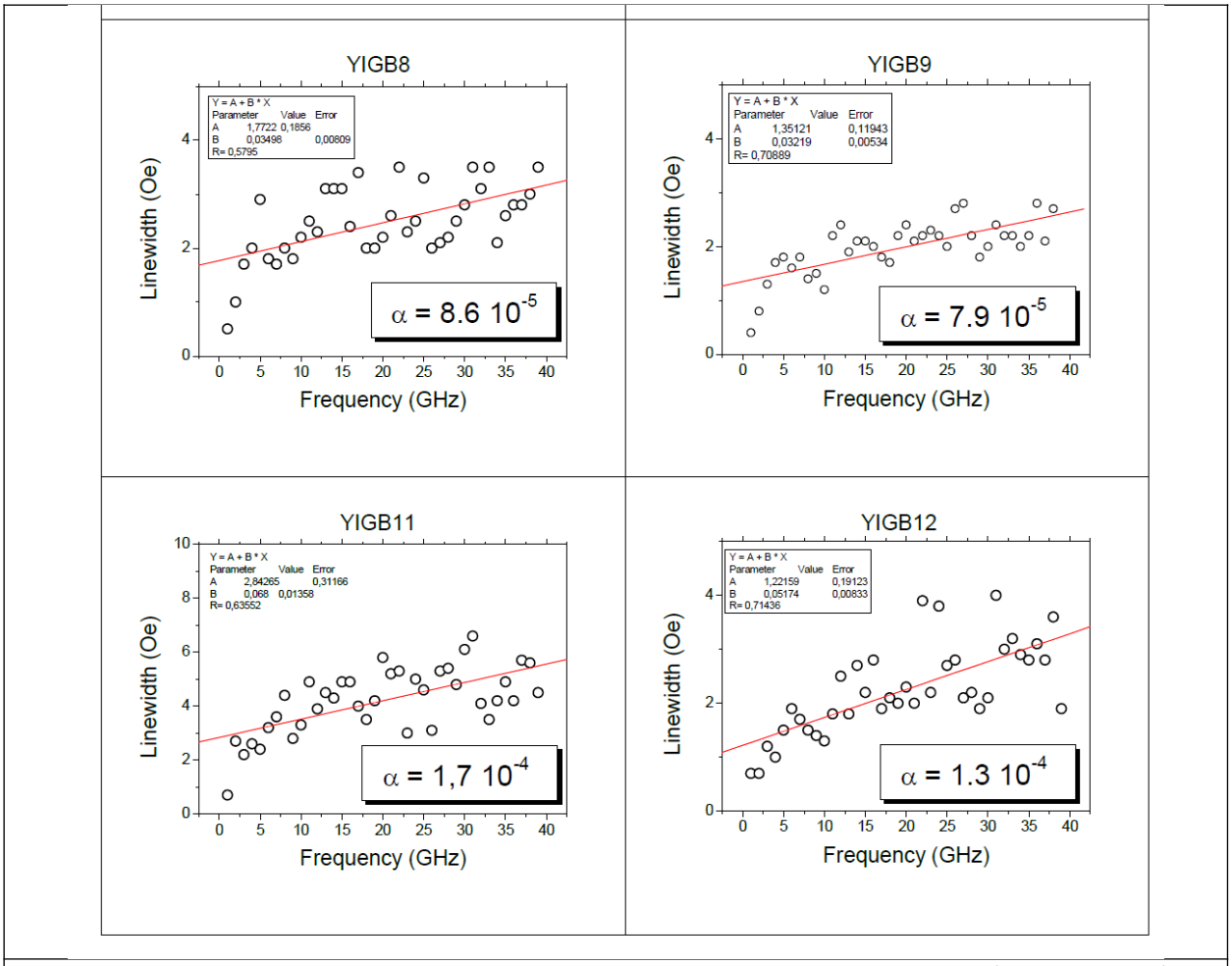

Figure 2: FMR-linewidth characterizations for different $Bi_xY_{3-x}IG$ films. The nominal Bi content is x=0.1 (YIGB8 and YIGB9) and x=0.2 for (YIB11) and (YIGB12). We observe about a factor of 2 increase in the Gilbert damping upon x=0.2 Bi substitution. Yet, the damping stays in the low 10^{-4}.

The overall results point to the fact that, unexpectedly, doping does not significantly improve the signal to noise ratio. When using blue laser, this improvement is 50% (x1.5) for 0.1 Bi/f.u and 100% (x2) for 0.2 Bi/f.u.. However, when switching to the green laser which is the preferred BLS configuration, pure YIG film shows a larger signal than that of Bi doped one (Figure 3).

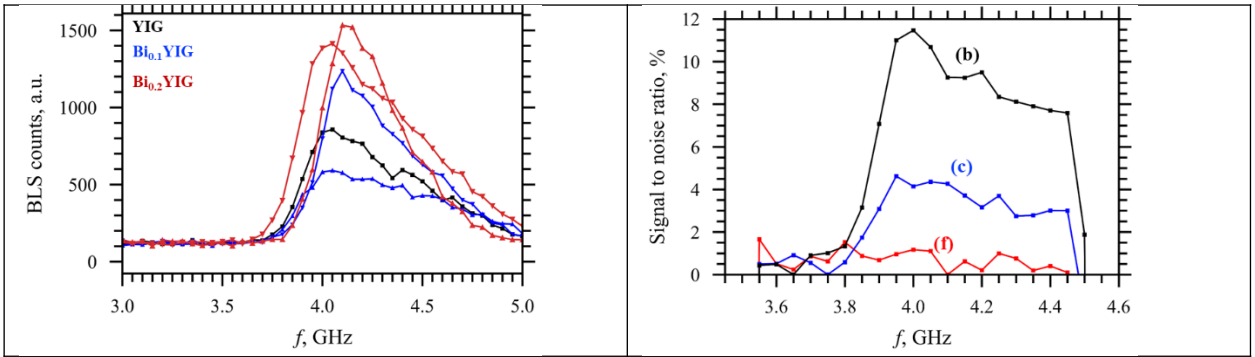

Blue laser | Green laser

Figure 3: left panel: Blue laser μ-BLS signal comparison between YIG and BiYIG films with different bismuth content, showing the moderate improvement of the signal for Bi substituted films. Right panel (same colour code as in the left panel) showing that Bi substituted samples have a worse signal to noise ratio than the pristine YIG film using a green probing laser.

Conclusion: The studied Bi substitution does not lead to a significant improvement of the BLS signal to noise ratio when using a blue laser and is even detrimental when using a green laser. As a consequence we decided to not explore further this path and resolved to work with YIG film using the blue laser configuration.

As for a possible explanation of the obtained results, we can speculate that this is linked to the sign of Faraday rotation in pristine YIG and in Bi doped YIG. Those signs are opposite and have complex wavelength dependence; we can therefore attribute our results to a reduction of the overall Faraday rotation in the green wavelength leading to a smaller signal for Bi doped YIG than with pure YIG. This compensation seems less effective at the blue wavelength. However when the Bi content is much higher (1 Bi/f.u.) we recover the known behaviour with a large Faraday rotation with a worse damping and extrinsic linewidth.

3 DEVICE MICROFABRICATION STATUS

The devices design has been pursued to obtain a coherent set of data on the SW eigenmodes. This choice is relevant as the different techniques that will be used within k-NET (MRFM, BLS and VNA) have non-overlapping capabilities and will deliver complementary information. By maximizing completeness of the k-space mapping, a more reliable and accurate theoretical modelling (WP3) can be reached. Given the risk of slight variations from sample to sample of the magnetic properties and in particular the Gilbert damping parameter, we decided that the three spectroscopy techniques should be conducted on the same garnets films. Requirements for such devices are:

- high quality fabrication of YIG microstructures.
- interfacing such microstructures with radiofrequency excitation-detection circuitry.
- the microfabrication process does not deteriorate the dynamical properties of the magnetic elements.

We resolved to work with pristine YIG samples whose Gilbert damping is $<10^{-4}$ and with relatively large thicknesses (66 nm) so to have access to a rich eigenmodes spectrum. To simplify modelling and to avoid non-homogeneous magnetic configuration states, the selected shape is a disk. Different YIG disks diameters have been selected 0.5, 1, 3 and 5 µm. Those diameters will allow exploring different densities of k-space modes; this density is expected to grow (non-linearly) with disk diameter. Once the disks are etched down, metallic Au/Ti antennas will be evaporated. Ti provides adhesion of the antenna. However Ti is known to modify the stoichiometry of oxide surfaces thorough the formation of Titanium oxides. Such modification will negatively impact the YIG damping. We have developed an ALD encapsulating approach that allows to efficiently protect the YIG using a 10 nm thick HfO_2 layer (see Step 1).
The designs include devices for MRFM, VNA and µ-BLS experiments:

3.1 Device designs for MRFM experiments

MRFM is a near field technique in which a magnetic probe attached at the end of a soft cantilever is used to mechanically probe SW dynamics in nanostructures thanks to the dipolar interaction. Sample design includes an excitation antenna that is fabricated on the top of few YIG disks. The disks are spaced so that dipolar interactions between them are negligible.

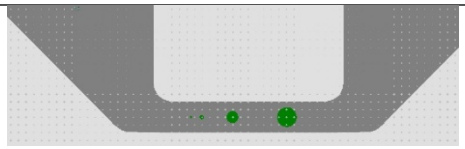

Figure 4: device mask layout for MRFM, from left to right YIG disks of 0.5, 1, 3 and µm in diameter covered with a strip radiofrequency antenna to excite magnetization dynamics. In this scheme with a single antenna the magnetic rf field is transverse to the antenna strip

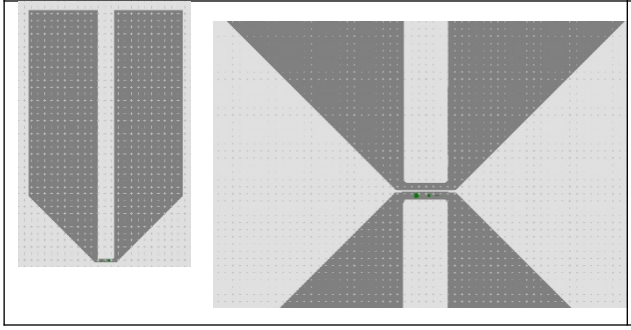

Figure 5: overview of the device mask layout of a single antenna design that enables to apply the magnetic field in one direction and a double antenna design that allow to combine independent in-plane and out-of-plane radiofrequency fields. The gap between the antennas is 2µm

3.2 Device designs for µ-BLS

µ-BLS measurements are performed by collecting inelastically scattered photons. Given that the disks will be covered by a thick metallic layer, probing the sample will need to be performed from the back-side of the substrate. This experimental configuration allows for higher flexibility compared to MRFM spectroscopy as rf-contacting is performed using wire bonding in close proximity to the disks. A larger number of designs are selected. Each µ-BLS cell includes 3 designs. A first design common to all cells where 4 disks with diameters of 0.5, 1, 3, 5 µm are fabricated under the center conductor of a shorted S-G-S antenna. A second design is based on radial field excitation based on an Omega shaped antenna. Its goal is to give access to modes excited by non-uniform rf fields. A third design allow for both, in-plane and out-of-plane excitation fields.

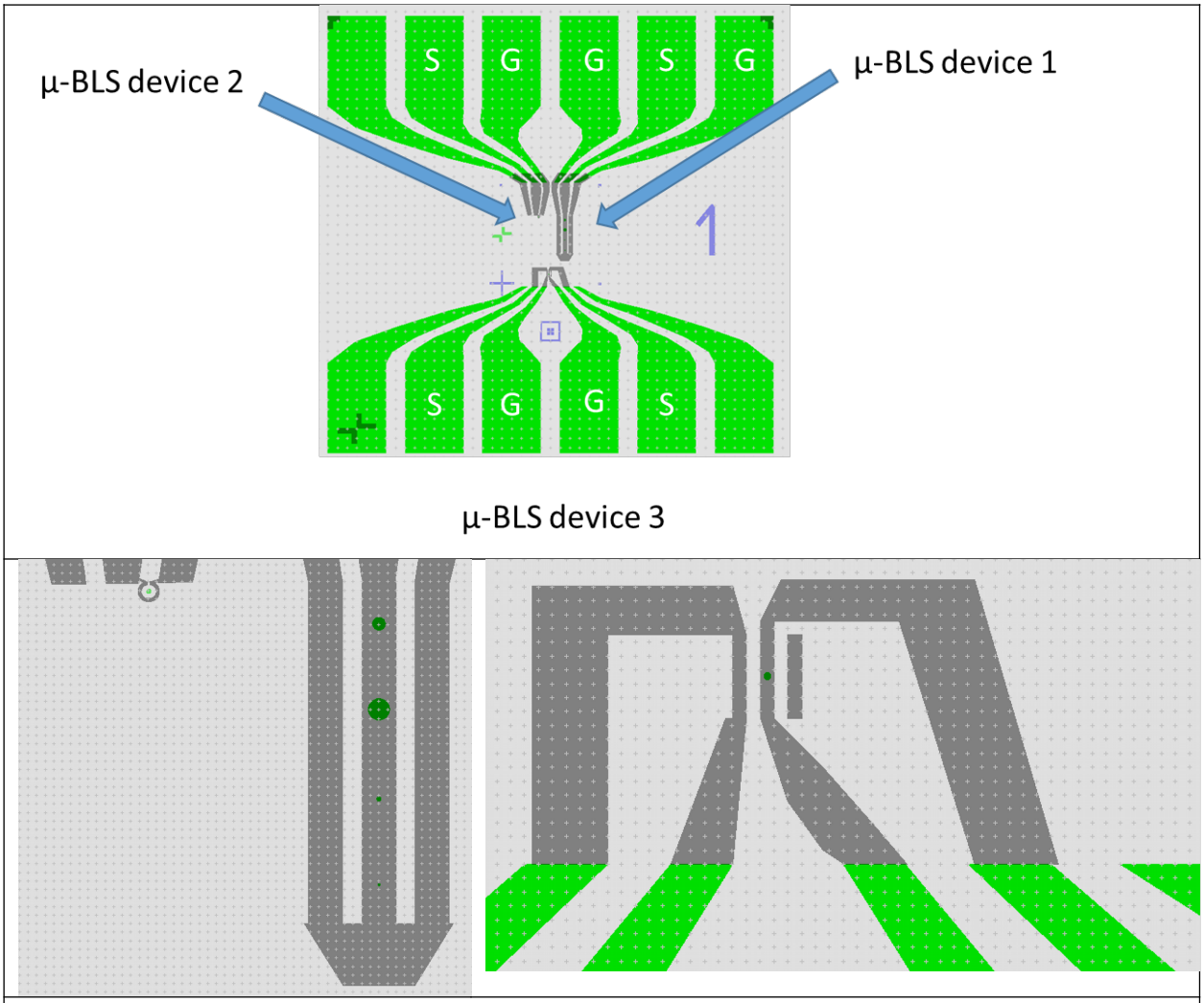

Figure 6: layout of a typical µ-BLS cell, device 1 is where 4 disks with diameters of 0.5, 1, 3, 5 µm are fabricated under the centre conductor of a shorted S-G-S antenna. Device 2 second design is based on radial field excitation based on an Omega shaped antenna. Device 3 allow for both, in-plane and out-of-plane excitation fields. Bottom panels are zoom on the active area where the YIG disks are pictured in dark green.

3.3 Device designs for VNA experiments

Unlike µ-BLS or MRFM, VNA measurements do not have any spatial resolution, as a consequence, it is not possible to share rf circuitry among many disks. Each YIG disk should therefore have a dedicated excitation/detection antenna. VNA measurement requires a probe setup as S-parameters calibration needs to be performed as close as possible from the disks to improve sensitivity and accuracy. We have implemented a design provided by partner CNRS-C2N that has been optimized during previous studies and adapted it to the requirements of k-NET. Rf-probes with a 150 µm pitch will be used on such devices.

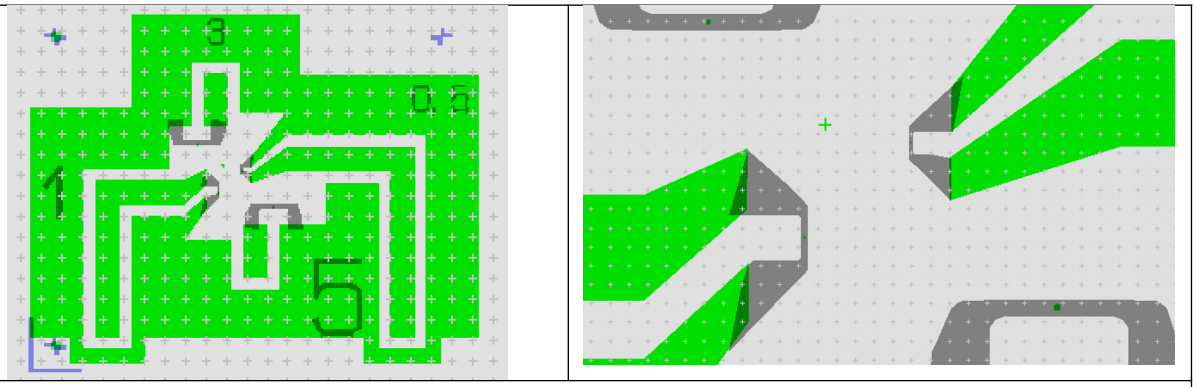

Figure 7: Design layout for the VNA characterisation, there is 4 landing areat for 150 µm G-S-G rf tip. The right panel shows a zoom on the central area.

3.4 Fabrication steps

Step 1: ALD encapsulation of YIG

We use atomic layer deposition of Hafnium oxide (HfO_2) to cap the YIG surface. Requirements are conformal growth a thin the oxide layer. We selected a thickness of 10 nm using an Ozone based process at 100°C. Upon HfO_2 deposition, broadband FMR measurements have been conducted and reveal that there is no effect of the deposition process on the YIG layer dynamical properties.

Step 2: alignment marks fabrication

Alignment marks have been defined using a e-beam lithography. PMMA A4 resist has been used to lift-off Ti(10nm)/Pt(40nm)/Ti(40nm) alignment marks. The objective of having top 40 nm thick Ti layer is to protect the Pt layer during the IBE etching process of step 3.

Step 3: Disk definition

An electron beam writing process based on a negative resist (MAN 2400) has been used to define the disks. Subsequently etching using an IBE has been conducted. During the IBE process (at 350V acceleration voltage and 0.5 mA/cm^2 beam fluence) the temperature is cooled down to 5°C. Resist has been removed using acetone. AFM characterisations show that the process has been successful for most disks. There is however evidence for material redeposition on the resist edges that should not impact the devices performances.

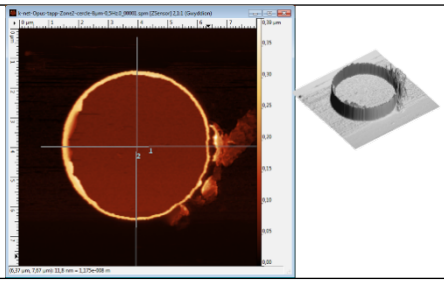

Figure 8: AFM pictures (in 2D and 3D) of a 5µm diameter disk showing the perfect circular shape but also the edge redeposition on the resist flanges

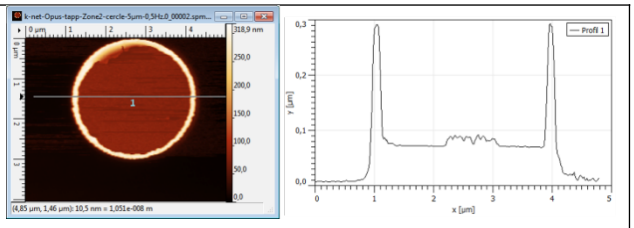

Figure 9: AFM pictures (in 2D) of a 3µm diameter disk showing the perfect circular shape but also the edge redeposition on the resist flanges visible on the line-cut as two sidewalls of about 200 nm in height.

Step 4: Electrode deposition

An electron beam writing process has been used to define the high resolution part of the rf circuitry. The e-beam resist PMMA-A6 has been used. The A6 resist has thickness of 400 nm and allows defining 200 nm thick Ti\Au electrodes using a lift-off process. Such thickness is necessary for 50 Ohm impedance matching.

Step 5: Connection pads fabrication

At this date this step is not yet implemented, we intend to use e-beam lithography with large writing current and PMMA A6 resist. This will be the last fabrication step.

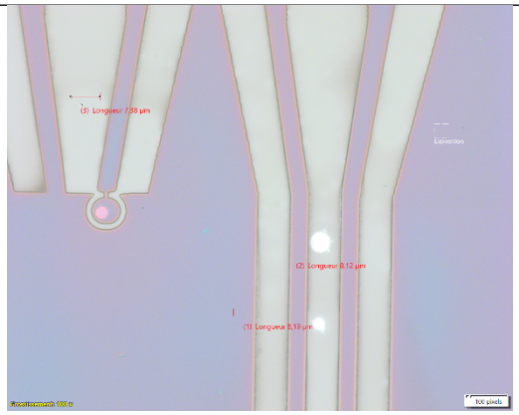

Figure 10: Optical microscopy image of device 1 and 2 of the µ-BLS design, prior to metal deposition. The disks are aligned with respect to the electrodes

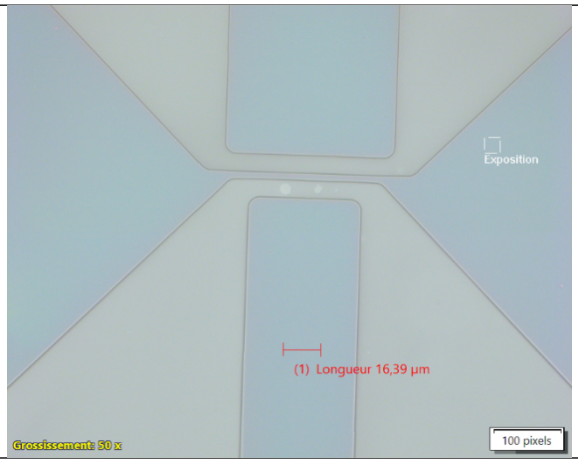

Figure 11: Optical microscopy image of MRFM design, prior to metal deposition. The disks are aligned with respect to the electrodes.

4 CONCLUSION AND OUTLOOK

Fabrication of first devices generation has been successfully implemented. This work has allowed us to identify roadblock in the fabrication process of the second generation devices that will include dynamic-al control of the magnetic losses using the spin-orbit-torque generated in a Pt over-layer. The use of MAN resist is not to be continued to avoid edge redeposition during IBE. A hard mask using Pt/Al layer will be developed.